2.2 CHARACTERIZATION OF THE MICROSTRUCTURE AND TEXTURE OF NFA-1 FOR TWO DEFORMATION PROCESSING ROUTES -- S. Pal, M.E. Alam, G. R. Odette (UCSB), J. Lewandowski (Case Western University) D. T. Hoelzer (ORNL) and S. A. Maloy (LANL)

OBJECTIVE

The objective of this research is to characterize the effect of different processing routes on the microstructural development and texture evolution of the FCRD-NFA-1alloy to facilitate the fabrication of component structures.

SUMMARY

Our previous investigation showed that NFA-1 produced through ball milling and hot extrusion followed by hot cross rolling suffers from severe micro-cracking on planes parallel to the plate surface and normal to the thickness direction. The microcracking inhibits fabrication of components, such as thin wall tubing, by conventional processing routes. This work reveals that a strong {001}<110> brittle texture component develops in NFA-1 during thermo-mechanical processing. Dislocation pile-ups at low angle boundaries result in formation of cleavage micro-cracks on {001} planes. In contrast, tubes formed by hydrostatic extrusion develop a strong {110}<211> "J_1-shear texture" component and low angle grain boundaries. Since preferred slip occurs on {110} planes in bcc Fe, deformation is readily accommodated by easy dislocations glide in the hydrostatic tube extrusion case. This is in contrast to {001} slip planes with pile ups that lead to stress concentrations and micro-crack nucleation in the extruded and cross rolled plate.

PROGRESS AND STATUS

Introduction

A nanostructured ferritic alloy (NFA), called FCRD NFA-1, was processed and is being qualified as part of collaboration between UCSB, LANL and ONRL [1-2]. Processing the plate involved a series of steps, including: 1) ball milling to produce powders with dissolved Y, Ti and O; 2) consolidation by hot extrusion at 850°C that also precipitated nano-oxides; and, 3) annealing and cross rolling at 1000°C. Following steps produce the base material, in the form of a plate, which is later used as a starting material for the thin wall tube formation through cold working process, such as pilgering. Presence of severe micro-cracks in the through thickness direction of plate, shatters the whole component during tubing by propagating along the radial direction of the tube. Very recently, hot hydrostatic extrusion method has been employed to produce tube from this NFA-1 alloy at Case Western University. It is well reported that application of hydrostatic pressure can change the ductility and fracture behavior of a brittle monolithic metal [3]. Component fabrication from brittle intermetallic material such as NiAl was successfully carried out using hydrostatic extrusion method near to its brittle to ductile transition temperature [4]. Present study is a prelude to understand the microstructural development and texture formation; when, same NFA-1 alloy processed through two different routes, hot extrusion followed by cross-rolling and hydrostatic extrusion.

Materials and Methods

The nominal composition of NFA-1 is 14Cr-3W-0.4Ti-0.21Y-balance Fe. Hot consolidation results in precipitation of an ultrahigh density (order $5x10^{23}/m^3$) of Y-Ti-O nano-oxides (NO), primarily $Y_2Ti_2O_7$, with average diameters of 2-3 nm. These NO provide exceptional strength accompanied by high ductility, thermal stability and irradiation tolerance, including trapping helium in nm-scale bubbles at their interfaces.

The processing sequence described above resulted in a 12.5 mm thick plate that is characterized by pancake shaped grains. The grain size is taken as the average of the long (l) and short (s) dimensions d = (l + s)/2 and the grain aspect ratio as r = l/s. The plates also contain a high density of micro-cracks on planes parallel to the plate surface and normal to the thickness direction. The cross rolled plate (or as extruded bar) can, in principle, serve as the starting point for subsequent fabrication of NFA components.

However, the micro-cracks severely limit the conventional cold workability of NFA-1, and more generally similarly processed NFA [1, 2]. For example, tube processing typically involves multiple room temperature pilgering and high temperature annealing step sequences [5-7]. Very recently, hot hydrostatic extrusion was used to produce a small length of thin wall tubing from the NFA-1 plate with remarkable success [8]. Hot extrusion was performed two times with an area reduction ratio of 4:1, which is equivalent to 44% applied strain. An aluminum mandrel was used to promote uniform wall thickness and stable deformation. The final product is completely free from micro-cracking. This motivated in-depth characterization of the microstructure and texture of NFA-1, for both of these processing routes. The microstructure of the plate and hydrostatically extruded tube were observed by SEM, TEM on FIBed liftouts and EBSD were used to characterize the corresponding textures. The characterization studies led to a micromechanical hypothesis regarding formation of the microcracks. The plate and tubing reference directions and specimen orientation are schematically illustrated in Figure 1.

a)

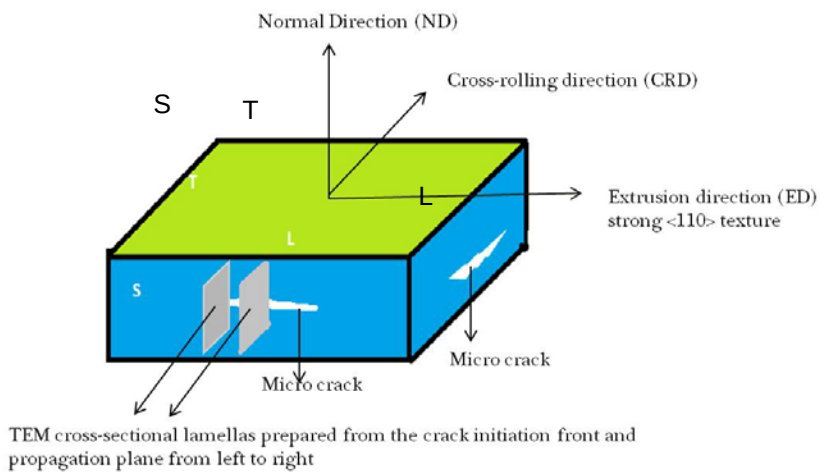

b)

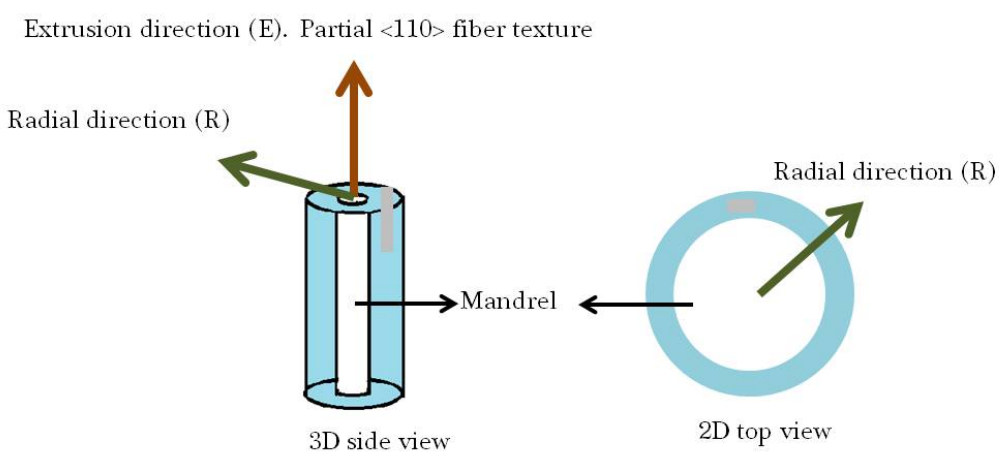

Figure 1. a) Schematic of a plate orientations referenced to the prime deformation directions. Micro-cracks, which are also shown in the image, run perpendicular to the short (S)-thickness direction. The tensile and cracked specimen orientation (L, T, and S) convention is also shown in Figure 1a. and, b) a schematic of the hydrostatically extruded tube showing the two key extrusion (E) and radial (R) directions. The region from where the TEM lamella is prepared is marked by grey box.

For cracks this convention is that the first letter defines the direction parallel to the front: L, T and S, and the second letter the direction of propagation. For tensile tests the letter defines the specimen axis. Planes and surfaces can also be defined in terms of L, T, S as parallel to the top (LT), side (LS) and front (ST);

Results

The two NFA-1 conditions characterized are: a) plates deformation processed by hot extrusion, annealing and cross rolling; and, b) tubes fabricated by hydrostatic extrusion. The hot extrusion, at Case Western University, was carried out starting with a gun drilled thick wall tube on a mandrel. The tube was taken from the cross-rolled plate with its axis in the extrusion direction. Therefore, it is very important to define the primary deformation orientations for both processing conditions by referencing physically relevant directions. Figure 1a shows a schematic of the plate, defining the longitudinal (L), transverse (T) and short (S) directions as labeled accordingly along with primary deformation extrusion (L) and cross-rolling (T) coordinate system. Figure 1b shows the two relevant radial and extrusion directions for hydrostatic processing.

Microstructural characterization by SEM

Figure 2a and b show SEM images for LS and LT views, respectively, of the NFA-1 plate. Grains are elongated in the extrusion direction in case of LS view. Black Ti/Y rich precipitates along with the micro-cracks are seen in the SEM image for the LS view in Figure 2a, No microcracks are found for the LT view shown in Figure 2b. In case of tube, Figure 3 shows the SEM image of the polished surface of the sectioned tube normal to the extrusion direction.

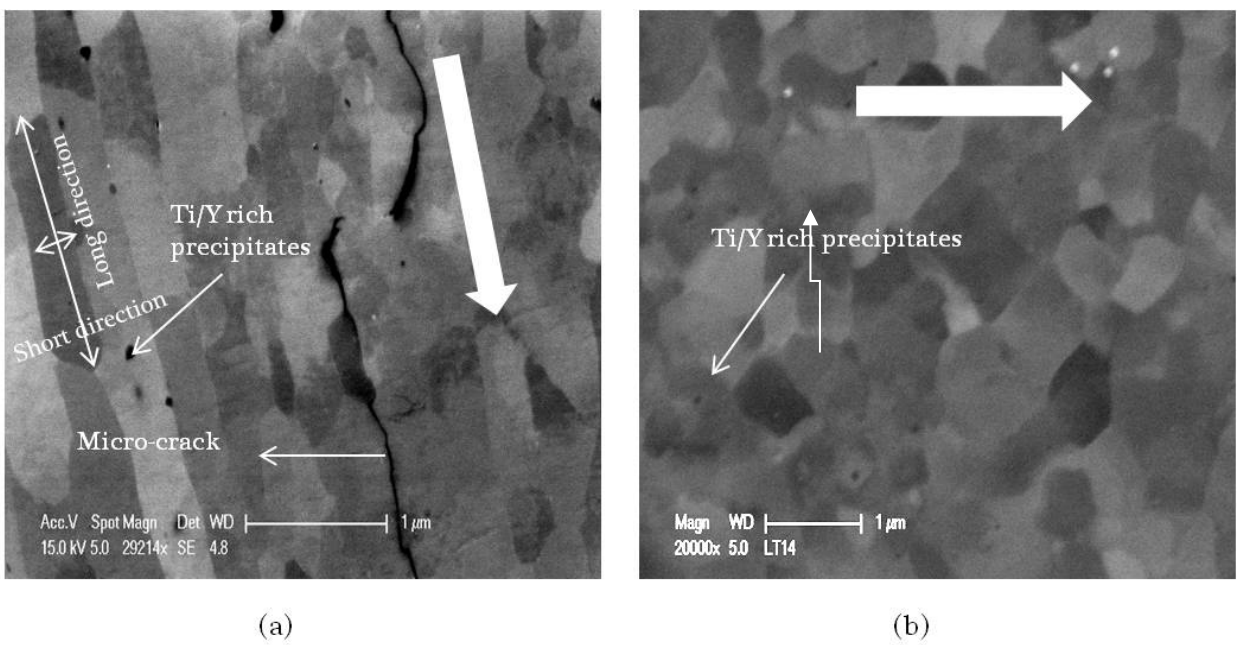

Figure 2. a) A SEM image for the LS view; b) a SEM image for the LT view. The large arrows mark the extrusion direction. Other components of the microstructure are labeled. The long and short dimensions of an individual grains are seen in the Figure 3a. The same method for grain size measurement is followed for the microstructural characterization of both tube and plate.

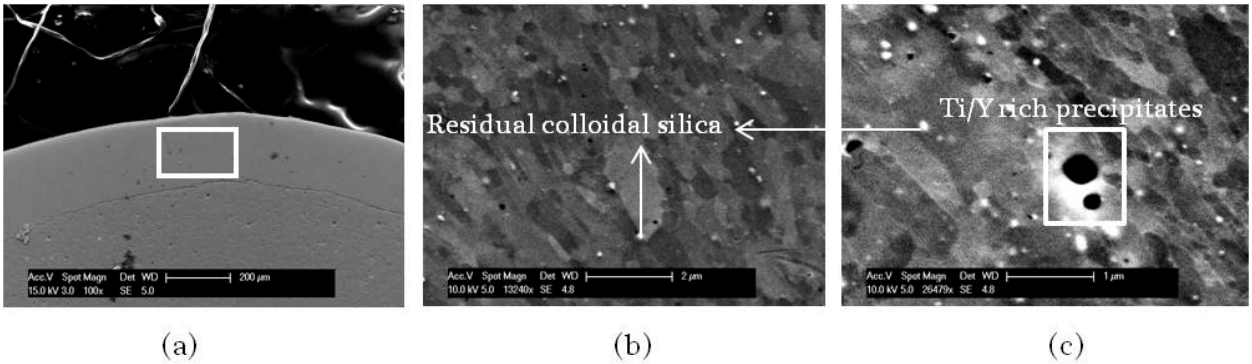

Figure 4. a) A low magnification SEM micrograph showing the tube wall cross section with the mandrel. The extrusion direction is normal to the image plane; b) a magnified view of the location marked by the white box in Figure 3a and, c) grains elongated in the radial direction (maximum sheer stress direction) of the hydrostatically extruded tube (see Figure 1b), where the dark particles are either Ti and Y rich precipitates, while the bright particles are residual colloidal silica.

The corresponding average grain sizes and standard deviations for the plane parallel to the top (LT) and side surface (LS) of the plate are summarized in Table 1. Here the grain size is taken as the average of the long and short dimension and the aspect ratio as the long divided by short dimension. The grains observed in the LS view parallel to the thickness direction have “flattened” shapes and are elongated along the observed extrusion direction. The grain size distributions and aspect ratio for the tube are also given in Table 1. The SEM micrographs of the tube section in Figure 3b and c reveal grains elongated in the radial direction. SEM images in Figure 2a and Figure 3c clearly show the plate’s side (LS) view, the contrast-orientation differences between the elongated grains are much stronger in comparison to the tube. Most notably, hydrostatic extrusion does not result in the formation of the microcracks.

Table 1. Showing the grain size and aspect ratio for the plate and tube conditions.

Sample surface	Average grain size (μm)	Grain aspect ratio
LT plane for plate	454 ± 142	1.2 ± 0.2
LS plane for plate	1077 x 397	2.7 ± 1.1
Cross-sectional plane for tube	590 ± 210	2.1 ± 1.1

Microstructural characterization by TEM

Figure 4a shows a SEM image of the tube cross-section indicating the location of a FIB lift out at a ≈ 45° angle to the radial, maximum shear, direction. The FIBed foil face is parallel to the extrusion direction as shown in Figure 4b.

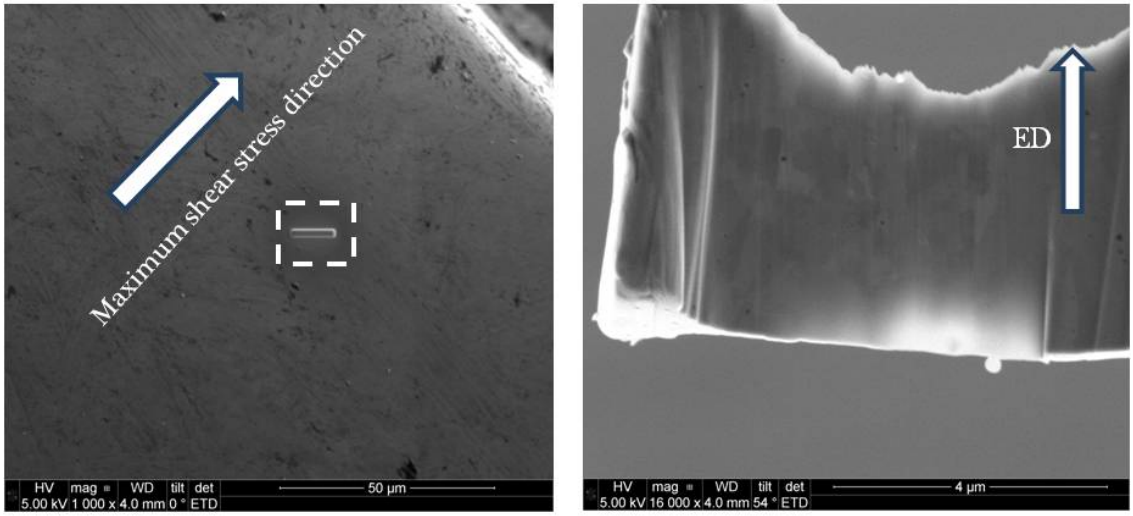

(a) (b)

Figure 5. a) The location of TEM lift-out for the tube; and, b) the corresponding FIBed TEM foil.

The bright field (BF) TEM images in Figures 5a to d clearly demonstrate that hydrostatically extruded tube contains a significant population of dislocations in the vicinity of a low angle boundary, marked in Figures 5c and d. The boundary between the grains, marked by the dashed box, is ill defined, with minimum contrast between the two sides, indicating a low angle character.

In order to accurately determine the grain sizes in the tube, the circled grain in Figure 6a is tilted in a two-beam condition (see Figure 6b) and the corresponding dark field image is shown in Figure 6c. The SAD pattern from the circled region using the smallest 20 µm aperture in Figure 6b, shows overlap of the near <111> grains, with only a small angle of misorientation. The corresponding dark field (DF) image in Figure 6c shows that all the bright grains are roughly equiaxed. These observations lead to the conclusion that low angle grain boundaries exist in what appear in BF to be elongated grains. This also confirms our SEM observation of grains elongated along the radial direction of the tube with a minimal contrast between grains of either side of the boundary, as shown in Figure 3b and c. Both SEM and TEM observe a similar average small grain diameter of ~ 0.5 µm.

Figure 7 show BF and DF TEM images of the plate side LS view, where the foil area is perpendicular to the extrusion direction. Figure 7a shows that microcracks track the elongated grain with lengths of ~ 0.4 ± 0.1 and ~ 3± 1 µm along the short and elongated directions, respectively. The plate condition contains a high dislocation density. SAD patterns, at a 0° tilt, are shown in Figures 7b and c, for the two circled regions in Figure 7a. The SAD patterns show the two bcc <110>-zone axis are only slightly misoriented with respect to each other. The DF image in Figure 7d shows a trans-granular crack propagating through a (001) grain (the corresponding (002) spot is marked in Figure 7b with a white circle). The BF image shown in Figure 7f is for a <110>-zone axis. These results show that, in contrast to the tubing, in the NFA-1 plate condition, elongated grains are separated by high angle boundaries.

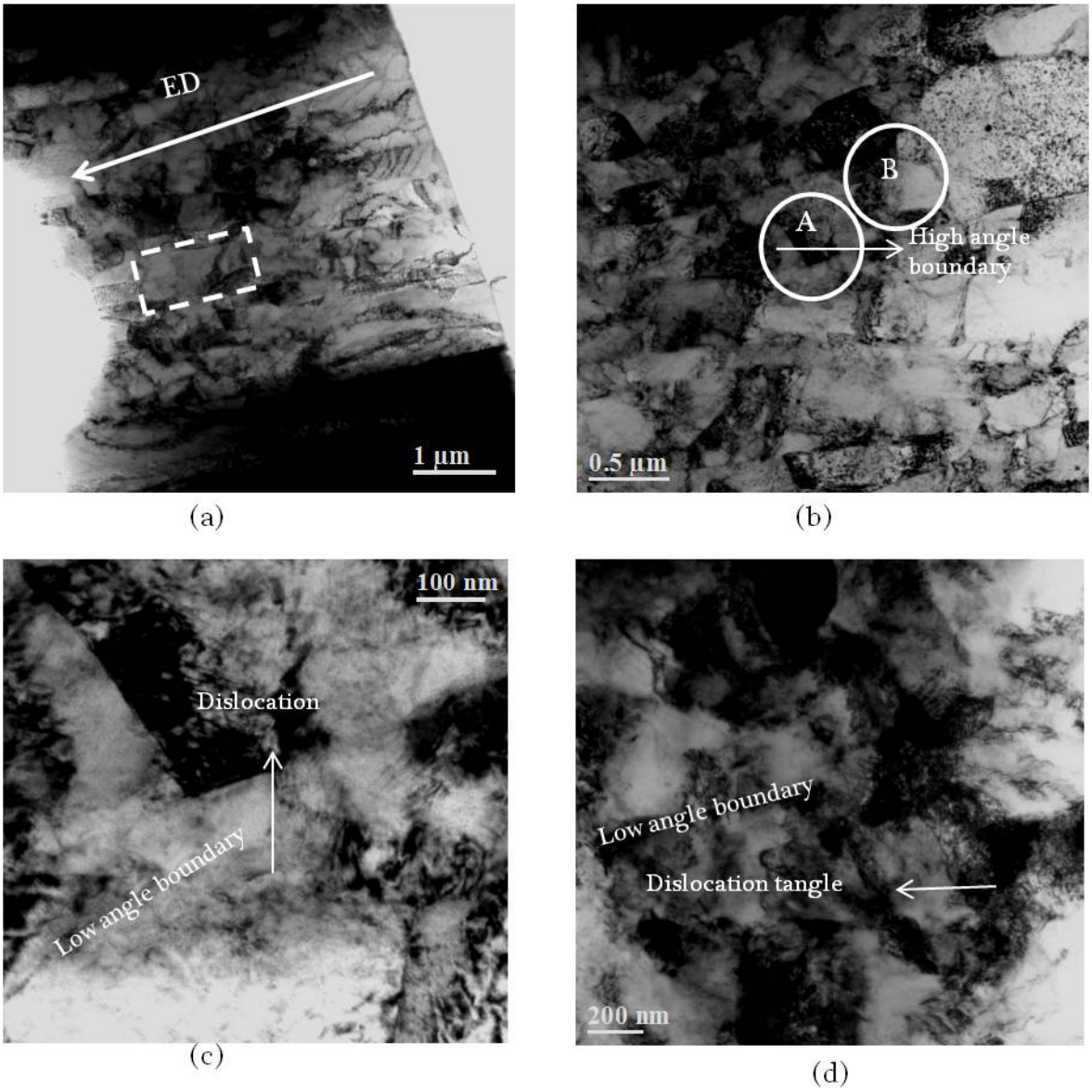

Figure 6. A bright field image of the tube microstructure at different magnifications:. a) the extrusion direction elongated grain structure; b) a high angle grain boundary; c) a magnified view of region marked as (A) in Figures 5b; d) a magnified view of region marked as (B) in Figure 5b showing low angle boundaries and dislocations tangles.

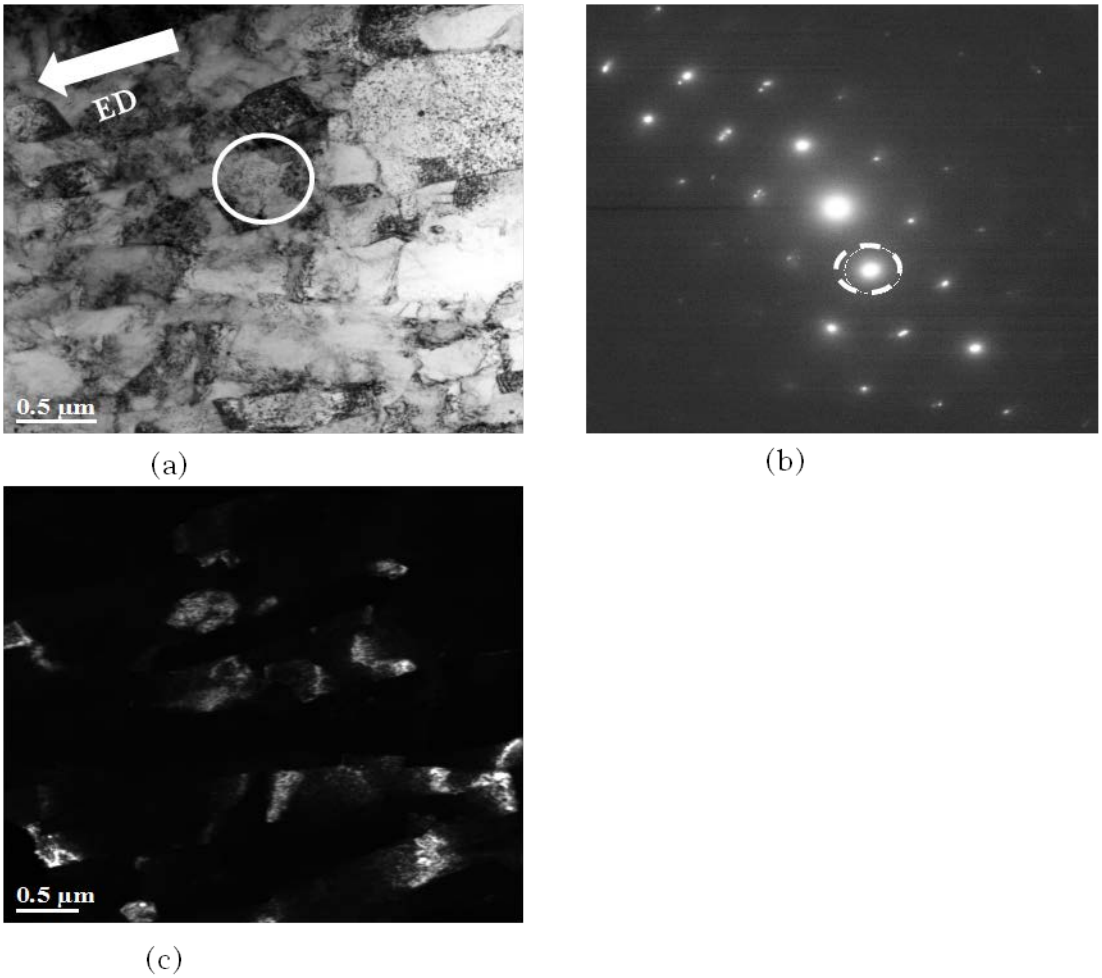

Figure 7. a) BF image of the tube microstructure; b) the SAD pattern for the circled region along the <111> zone axis under two beam conditions with the (110) bright spot circled; and, c) the dark field image of the (110) spot

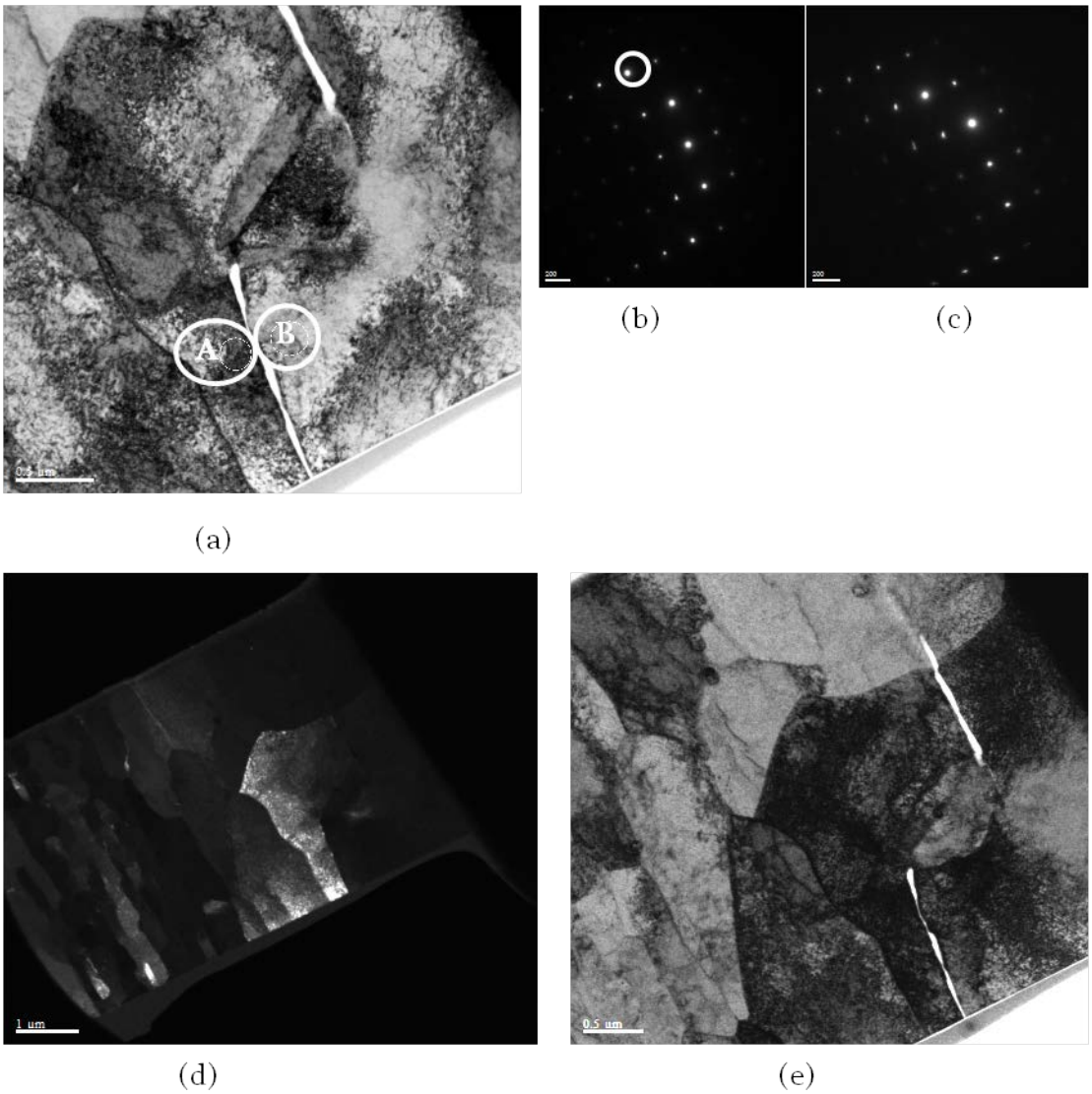

Figure 8. a) shows the BF image of the LS sample; b) and c) are the SAD patterns from the circled regions in a; d) a DF image from the circled SAD spot in Figure 6b; and, e) a BF image for a<110> zone axis.

Texture Characterization by EBSD

Texture measurements for both the NFA-1 processed conditions were carried out by EBSD. For the plate, EBSD was carried out on both the side-parallel (LS) and top-parallel (LT) views (as shown in the schematic Figure 1a). Pole figure (PF) maps for the LT and LS parallel surface planes are shown in Figure 8. The PF show that the plate contains strong α-fiber texture along the extrusion direction with a partial α-fiber along the cross-rolling direction. A prominent <100>-texture component is observed in the direction normal to LT parallel surface planes.

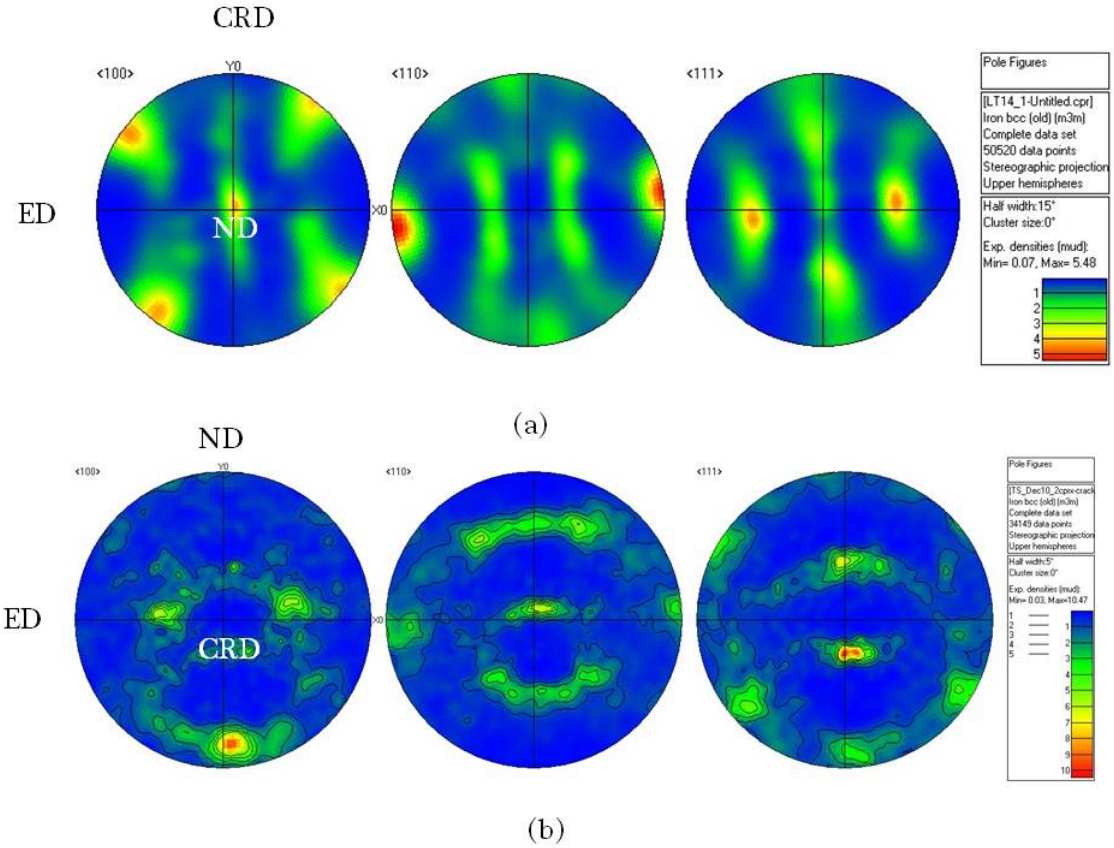

Figure 9. a) LT, and b) LS views: EBSD <100>, <110>, <111> poles of the plate sample, respectively. Equivalent deformation directions for the plate are also shown in the PF respectively by following the convention defined in Figure 1a and following text.

Texture measurements were carried out on a polished surface shown in the Figure 3a, normal to the extrusion direction. The texture of the tube is quite different compared to the plate as shown in Figure 9. The tube has a partial α-fiber texture in the extrusion direction.

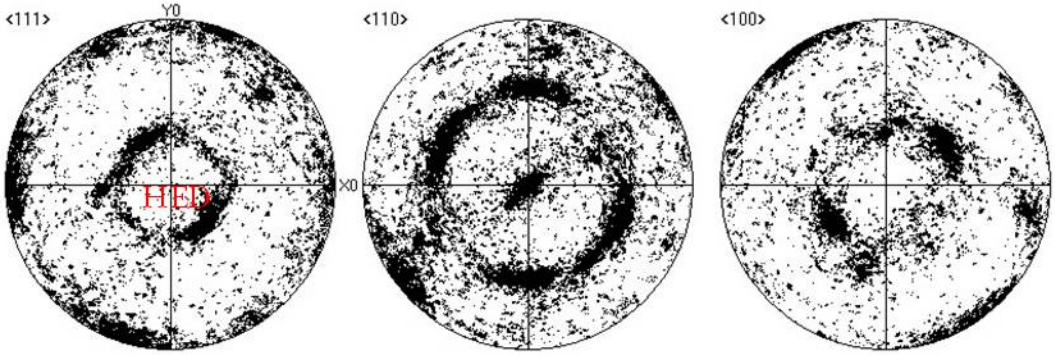

Figure 10. Pole <111>, <110>, <100> poles figures of the tube. Hydrostatic extrusion direction for the tube, schematically shown in Figure 1b, is also marked in the <111> pole figure of <111> pole.

PF analysis shows development of α-fiber along the extrusion direction for both the tube and the plate, while for the direction normal to the plate surface parallel planes and tube radius, the texture components are <100> and <111>, respectively. This observation is further corroborated in the inverse pole figures (IPF) in Figure 10, which show density of pole projections on a stereographic triangle with <001>, <110> and <111> vertices for the plate in the prime deformation directions.

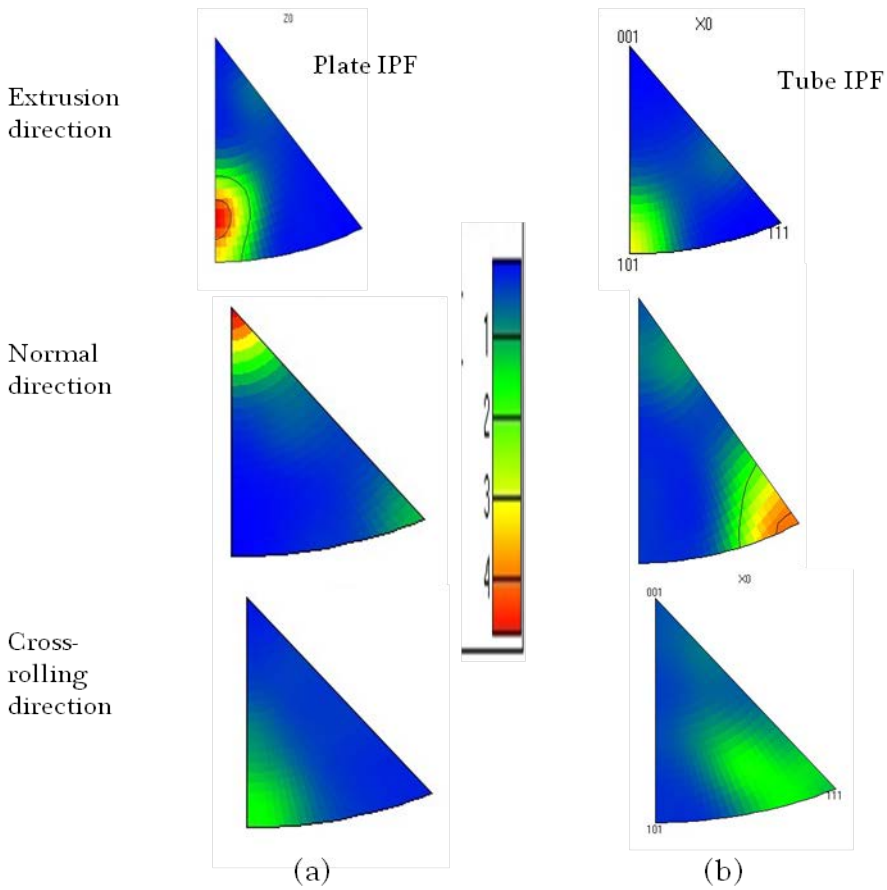

Figure 11. IPF maps of the tube and plate: a) the plate IPF for extrusion, surface normal and cross-rolling directions following the convention in Figure 1a; b) the tube radial direction, which is equivalent to the both cross-rolling and normal directions for the plate (see Figure 1b.) The extrusion direction is the same for both tube and plate.

The IPF analysis clearly demonstrates that while along the extrusion direction texture is similar for both the tube and plate, it differs in the normal direction: a strong <100> in along the normal direction for the plate, and <111> in the normal radial direction for the tube. The latter is also the direction of the maximum sheer stress in the case of the hydrostatic extrusion.

PF and IPF maps are basically a 2D stenographic projection of either crystallographic directions or the deformation directions for the plate or tube. A fully accurate description of the texture and its components is not possible using PF or IPF plots. A more accurate way of representing texture requires an orientation distribution function (ODF) analysis. All the possible orientations in a sample are projected in a 3D Euler space (defined by three Euler's angles of, ϕ, ϕ_1 and ϕ_2) as shown in Figure 11. Preferred orientations produce a high-density region around a certain combinations of these angles. Figure 12a shows a 3D ODF plot created from the PF data using the series expansion method [9]. For the ease of visualization, 2D sections of the 3D cube containing ϕ and ϕ_1 from 0 to 90° for constant value of ϕ_2 is shown in Figure 11.

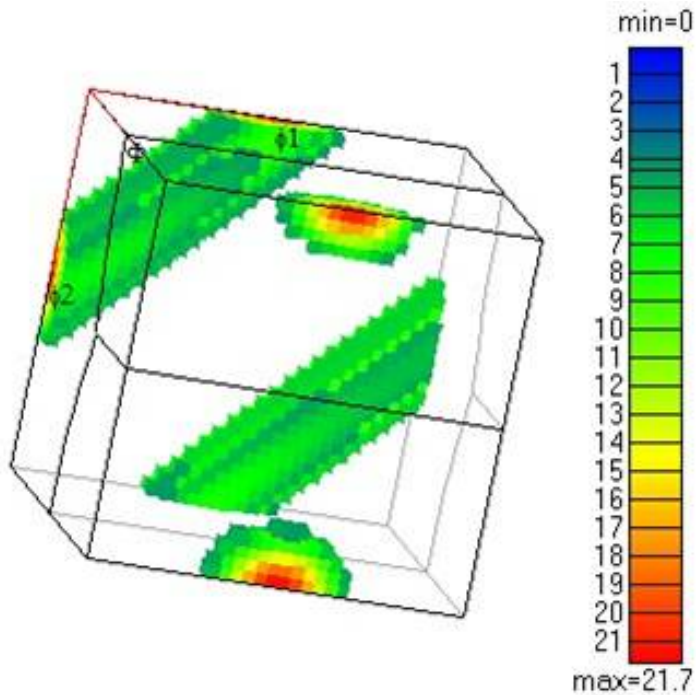

Figure 12. A 3D ODF plot for the plate.

The most important texture components for bcc steels occur at ϕ_2 = 0 and 45° sections [8], which are shown in Figures 12a, d and 12b,f for the plate and tube, respectively. Figures 12c and f show the ideal texture components for bcc steels (reproduced from Ref. [8]). These sections show the texture is completely different in the plate versus the tube. These ODF maps are compared with ideal ϕ_2 = 0 and 45° sections of bcc steel [8] shown in Figures 12c and f.

The texture components in the plate and tube are also shown on the ideal ODF plots as brown circle (plate) and blue box (tube), respectively. Notably the plate contains strong {001} <110> brittle cleavage texture components. Note, the PF and IPF analysis mainly showed a <110> α-fiber in the plate. However, the ODF analysis shows that α-fiber family contains three strong texture components: {001}<110>, {112}<110>, {111}<110>, with {001} <110> being by far the most dominant. Again, the {001}<110> α-fiber texture is also the most brittle cleavage system in bcc iron. This partly explains the origins of microcracking on (001) planes in the plate. The texture of the tube is quite different with dominant

components of {011}<211> and a lower fraction of {011}<111>. These two components belong to the ζ-fiber texture family as shown by the brown line in Figure 12c.

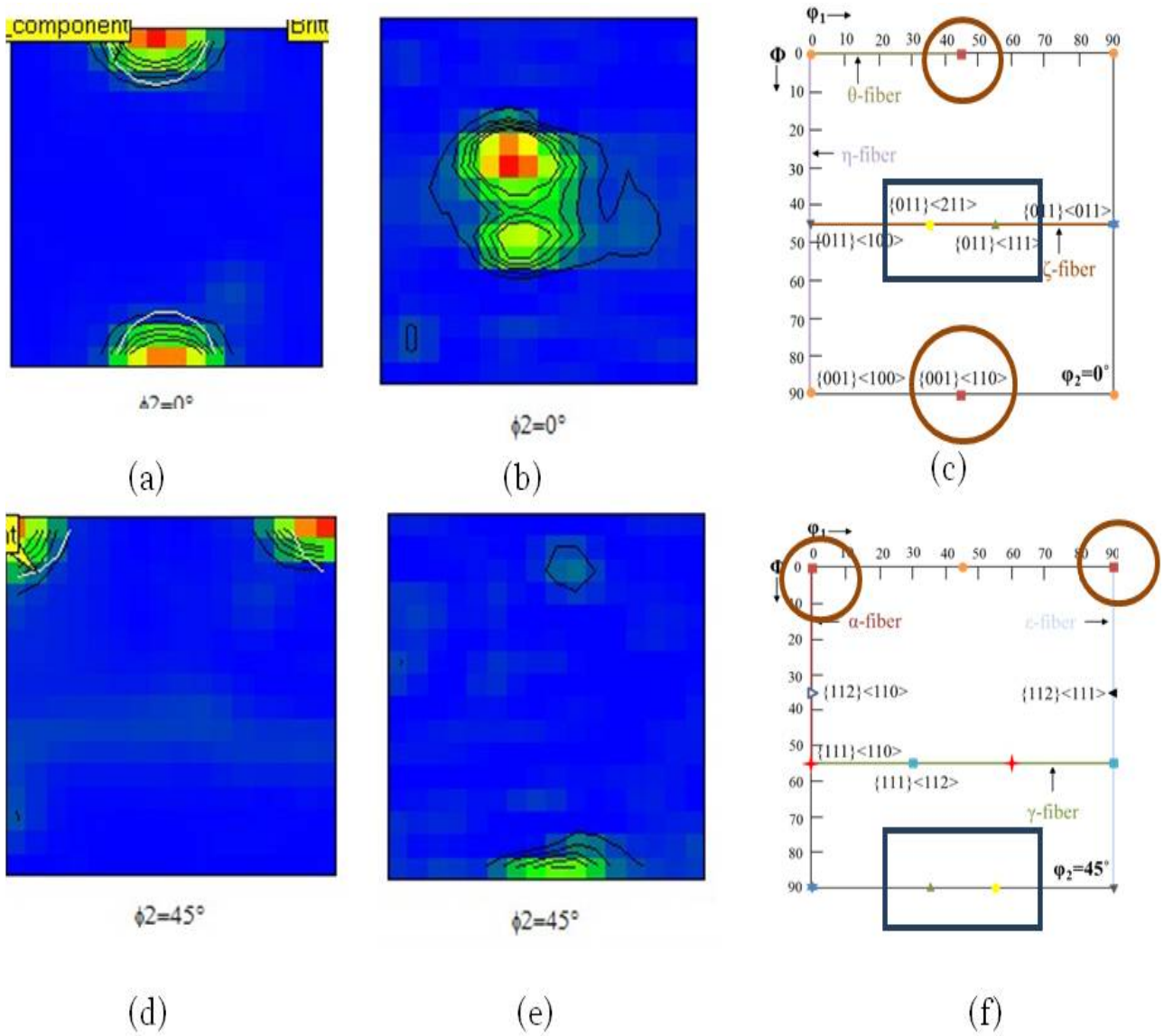

Figure 13. a), b) and c) (top) are ϕ_2 = 0 sections for the plate, tube and ideal ODF texture components for bcc steel, respectively [8]. Figures 12 d), e) and f) (bottom) are for the corresponding ϕ_2 = 45° section.

Conclusions

- Various characterization methods have been used to explore the microstructures and crystallographic textures that develop in NFA-1 under two deformation processing paths.
  In the case of the hot extruded and cross-rolled plate, the grains are elongated along the extrusion direction and a strong α-fiber texture develops along with a brittle cleavage {100} <011>-fracture system. This restricts glide on {100} planes lead to dislocation pile ups and stress concentrations with increasing strain, resulting in formation of corresponding population of micro-cracks.

- In case of hydrostatic extrusion of tubes, the grains are elongated along the maximum sheer stress direction and develop corresponding sheer texture components of {110} <112> and {110}<111>. Deformation occurs on {110}-bcc easy glide planes and is accompanied by formation of low angle sub grain boundaries. These microstructures and textures are not brittle, hence, cracking is not observed in the hydrostatically extruded tube.

Acknowledgments

This work is part of a multi-laboratory collaboration between LANL, UCSB and ORNL. The DOE Office of Fusion Energy Sciences partially supported the research reported here. NFA-1 was produced under the sponsorship of the DOE Office of Nuclear Energy through both a NEUP grant and the FCRD program.

References

[1] G.R. Odette, “Recent progress in developing and qualifying nanostructured ferritic alloys for advance fission and fusion applications”, JOM, Vol-66, Number-12, 2012, 2427-2441.
[2] M.E. Alam, N. J. Cunningham, D. Gragg, K. Fields, G. R. Odette, D. T. Hoelzer and S. A. Maloy**,** **“**Mechanical Properties Characterization of a Larger Best Practice Heat of 14YWT NFA1**”**, Fusion Reactor Materials Program, June 30, 2014, *DOE/ER-0313/56 – Volume 56.*
[3] J.J. Lewandowski and P. Lowhaphandu, **“**Effects of hydrostatic pressure on mechanical behaviour and deformation processing of materials”, International Materials Review, 43(4), (1998), 145-187.
[4] J.J Lewandowski, B. Berger, J.D. Rigney, and S. N. Patankar, "Effects of Dislocation Substructure on Strength and Toughness in Polycrystalline NiAl Processed via High Temperature Hydrostatic Extrusion", Philosophical Magazine A, 78 (3), (1998), 643-656.
[5] S. Ukai, “Perspective of ODS alloys application in nuclear environments”, Journal of Nuclear Materials, 307-311, (2002), 749-757.
[6] B. Leng, “Recrystallization texture of cold-rolled oxide dispersion strengthen ferritic steel”, ISIJ International, 51 (2011), 951.
[7] L. Toualbi, “Assessment of a new fabrication route for for Fe-9Cr-1W ODS cladding tubes”, Journal of Nuclear Materials, 442 (2013) 410-416.
[8] Un-published work – “Effect of tube processing methods on the texture and grain boundary characteristics of 14YWT Nanostructured Ferritic Alloys” - work carried out in LANL.
[9] H.J. Bunge, “Texture Analysis in Material Science: Mathematical methods”, Butterworths, London, p-323, 1982.